Wall Shear Stress and Pressure Fluctuations under Oscillating Stimulation in Helical Square Ducts with Cochlea-like Geometrical Curvature and Torsion*

Noëlle C. Harte[1,2], Dominik Obrist[1], Marco D. Caversaccio[1,2], Guillaume P.R. Lajoinie[3] and Wilhelm Wimmer[1,2,4]

Abstract—Our study aims to provide basic insights on the impact of the spiral shape of the cochlea, i.e., of geometric torsion and curvature, on wall pressure and wall shear stress. We employed computational fluid dynamics in square duct models with curvature and torsion similar to those found in human cochleae. The results include wall pressures and wall shear stresses within the ducts under oscillating axial flow. Our findings indicate that the helical shape generates higher transverse wall shear stresses compared to exclusively curved or twisted ducts. The wall pressures and transverse wall shear stresses we found rise to amounts that may be physiologically relevant in the cochlea.

Clinical relevance— The role of the spiral shape of the cochlea in hearing physiology remains, for a large part, elusive. For a better apprehension of hearing and its disorders, it is important to investigate the influence of geometric properties on biofluids motion and emerging phenomena in the cochlea.

I. INTRODUCTION

The cochlea, our organ of hearing, is a fluid-filled spiral structure that is small and difficult to access. Because direct experimental observations are limited, our understanding of hearing physiology remains partial. One unresolved question is that of the role and relevance of the cochlear morphology for hearing. In particular, the consequence of transverse flows on the shear flow along membranes has so far not been considered. In this study, we aim to quantify the effects of geometric curvature and torsion on wall shear stress and pressure fluctuations in abstracted models with cochlea-like geometric properties. In toroidal, twisted, and helical ducts, curvature and torsion cause transverse flow phenomena [1], [2], which further generate local pressure fluctuations and wall shear stresses [3], [4]. Using computational fluid dynamics, we simulated flow at oscillation frequencies covering the infrasonic regime and the low-frequency hearing range of humans, for which the apical region of the cochlea (the region with the highest curvature and torsion) is particularly sensitive.

The cochlea contains thin membranes, such as the basilar membrane (housing the sensory epithelium) and the Reissner's membrane (only consisting of two cell layers) [5]. Wall shear stress and pressure fluctuations caused by transverse flow could locally deflect these membranes. Our results could help to provide insights on the relevance of morphology for hearing.

II. METHODS

A. Duct Geometries

We have simulated fluid flow in straight, toroidal, twisted and helical geometries to independently characterize the impact of curvature and torsion on pressure fluctuations and wall shear stress (see top

row in Fig. 1). The geometries were constructed using established methods [1] with centerline curvature $\kappa = 1/3\,\text{mm}^{-1}$ and torsion $\tau = 1/8\,\text{mm}^{-1}$. These values approximate those measured in human cochleae [6]. To save computational resources, we chose a total arc length of the centerline of $10\,\text{mm}$ for all models, which is shorter than a human cochlea ($37\,\text{mm}$) [7]. The models' cross-section measures $2\,\text{mm} \times 2\,\text{mm}$ to capture typical dimensions of the cochlea [8].

B. Wall Pressure and Wall Shear Stress

The Cauchy stress tensor T is given by

$$\mathsf{T} = -p\mathsf{I} + \mathsf{S}, \tag{1}$$

where S is the viscous stress tensor, p is the pressure and I is the identity tensor [9]. We subtract the mean pressure $\bar{p}$ over the cross-section from the total pressure to obtain pressure fluctuations p_{fluc}:

$$p_{fluc}(x,y,z,t) = p(x,y,z,t) - \bar{p}(t). \tag{2}$$

S is computed using the symmetric part of the velocity gradient

$$\mathsf{S} = \mu[\nabla\mathbf{u} + (\nabla\mathbf{u})^T], \tag{3}$$

where $\mathbf{u} = \mathbf{u}(x,y,z,t)$ is the velocity field at a time t. The viscous stress $\boldsymbol{\tau}_w$ exerted by the fluid on a wall element with unit surface normal vector $\hat{\mathbf{s}}_n$ (pointing into the fluid domain) is

$$\boldsymbol{\tau}_w = \mathsf{S}\hat{\mathbf{s}}_n. \tag{4}$$

We can further decompose the viscous stress into an axial and a transverse component. We define the transverse component $\hat{\mathbf{s}}_{tr}$ as orthogonal to $\hat{\mathbf{s}}_n$ and to the duct centerline's tangent $\hat{\mathbf{t}}$:

$$\mathbf{s}_{tr} = \hat{\mathbf{s}}_n \times \hat{\mathbf{t}} \quad \text{and} \quad \hat{\mathbf{s}}_{tr} = \mathbf{s}_{tr}/\|\mathbf{s}_{tr}\|. \tag{5}$$

The local wall element coordinate system is then defined by $(\hat{\mathbf{s}}_{ax}, \hat{\mathbf{s}}_{tr}, \hat{\mathbf{s}}_n)$, with the direction of the axial component given by

$$\hat{\mathbf{s}}_{ax} = \hat{\mathbf{s}}_{tr} \times \hat{\mathbf{s}}_n. \tag{6}$$

Since $\boldsymbol{\tau}_w$ is perpendicular to $\hat{\mathbf{s}}_n$, we use the two-dimensional decomposition of the stress:

$$\boldsymbol{\tau}_w = \tau_{w,ax}\hat{\mathbf{s}}_{ax} + \tau_{w,tr}\hat{\mathbf{s}}_{tr}, \tag{7}$$

with axial wall shear stress $\tau_{w,ax} = \boldsymbol{\tau}_w \cdot \hat{\mathbf{s}}_{ax}$ and the transverse wall shear stress $\tau_{w,tr} = \boldsymbol{\tau}_w \cdot \hat{\mathbf{s}}_{tr}$.

C. Model Implementation and Numerical Model

The perilymph fluid in the cochlea is modelled as a Newtonian fluid and the flow is considered incompressible (low Mach number) [10]. We used a sinusoidal pressure boundary condition at the inlet and zero pressure at the outlet surface. The oscillation frequency f ranged from $0.125\,\text{Hz}$ to $256\,\text{Hz}$ (the human hearing range starts at $16\,\text{Hz}$). The associated Womersley numbers are $\alpha = \frac{d_h}{2}\sqrt{2\pi f \rho/\mu} = 1$ to 48, and thus cover quasi-steady to unsteady inertial flows (hydraulic diameter $d_h = 2\,\text{mm}$, dynamic viscosity and density of water at body temperature $\mu = 0.69\,\text{mPa\,s}$ and $\rho = 993\,\text{kg/m}^3$ [10]).

For the simulations, we used the finite element solver COMSOL Multiphysics® (COMSOL AB, Stockholm, Sweden). The meshes consist of $77\,500$ hexahedral elements per geometry, with ensured convergence. We determined the inlet pressure amplitude iteratively such that the axial velocity amplitude averaged over the cross-section W_0 remained $200\,\mu\text{m/s}$ across the stimulation frequency range [11], [12]. The resulting Reynolds number is $Re = d_h W_0 \rho/\mu = 0.58$, implying that the fluid phenomena are in the Stokes regime.

III. RESULTS

A. Wall Pressure

Fig. 1 shows the pressure fluctuations over time along the perimeter of a cross-section in the middle of the geometries.

In the toroidal duct, a pressure gradient between the outer ($\text{H} - \Phi$) and the inner wall ($\Upsilon - \Sigma$) of the duct can be observed as the result of fluid being pushed outwards. Notably, the pattern observed in toroidal ducts is unidirectional, i.e., it does not change with the direction of the axial flow. By contrast, in twisted ducts, the wall pressure changes according to the oscillation cycle of the axial flow. High wall pressure fluctuations arise in the proximity of corners. This observation agrees with Kheshgi's findings for steady flows [13]. The pattern remains consistent over the entire range of observed frequencies.

In the helical duct, we recover a combination of the patterns observed in the toroidal and the twisted
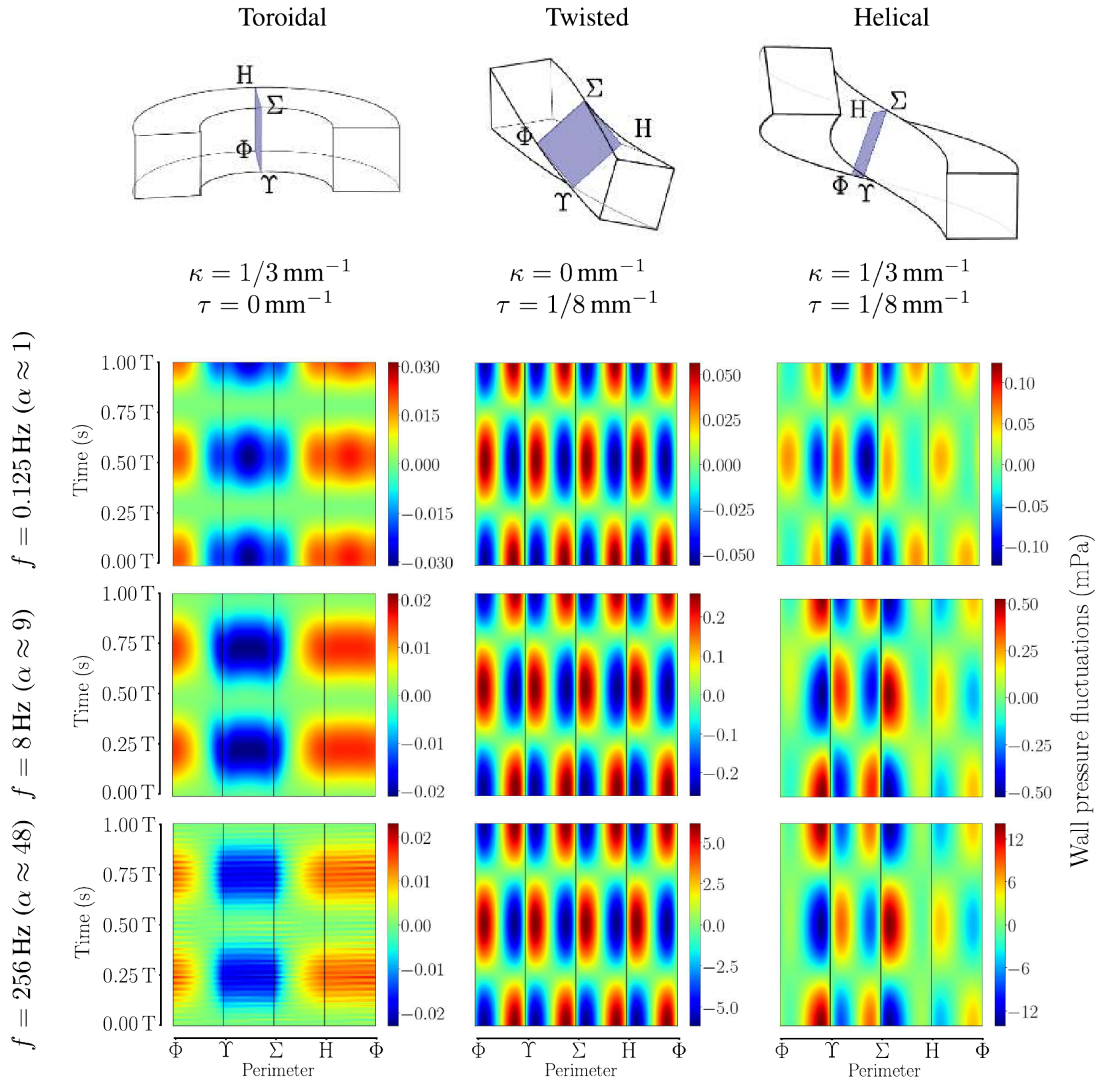
Fig. 1. Top row: Geometries with corresponding curvature κ and torsion τ. Greek capital letters indicate the corners of the central cross-section (shaded violet). Other rows: Pressure fluctuations along the perimeter of the central cross-section over time for different oscillation frequencies with period $T = 1/f$. Zero time in the plots corresponds to the time of maximum inlet pressure. Note that the pressure fluctuations at $\alpha \approx 48$ ($f = 256\,\mathrm{Hz}$) in the toroidal duct are distorted due to the proximity to the numerical noise floor (Fig. 2). The colorbars are scaled differently.

duct. At $\alpha \approx 1$, both contribute with comparable magnitudes, although the torsional effects dominate slightly. At higher α, however, the pressure fluctuations because of curvature decrease to negligible amounts. Notably, the pressure fluctuations reach greater magnitudes than the cumulative pressures observed in the other two ducts. The peak of the axial velocity is shifted toward the inner wall, because of the low Reynolds number and high curvature [14], and subsequently amplifies the pressure fluctuations near the inner wall.

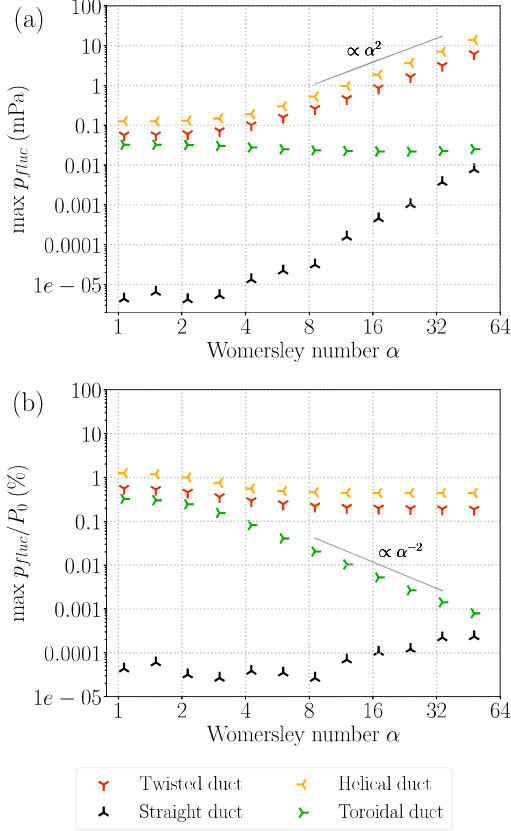Fig. 2a shows the maximum pressure fluctua-

Fig. 2. Maximum wall pressure fluctuations p_{fluc} (a) and p_{fluc} with respect to the inlet pressure P_0 in percent (b), as a function of the Womersley number. The black symbols indicate numerical noise defined as the maximum wall pressure fluctuations found in the straight duct simulations.

tion at the wall as a function of the Womersley number α. Since the inlet pressure amplitude P_0 was increased with the Womersley number to keep velocity amplitude W_0 the same, we examined the maximum pressure fluctuation with respect to P_0 in Fig. 2b. The maximum relative pressure fluctuations remain nearly constant for $\alpha => 24$ in the helical and twisted geometry, at a level of 0.4% and 0.2%, respectively. Surprisingly, the combination of curvature and torsion in the helical duct causes pressure fluctuations to increase more than twice as much as in the twisted duct, which has no curvature. In contrast, in the toroidal duct, the pressure

maximum is most pronounced at low frequencies and located at the center of the outer wall, whereas at high frequencies, the peak becomes wider and is distributed along the entire side wall (Fig. 1). We observed that the fluctuations decrease with α^{-2} for Womersley numbers $\alpha => 9$.

B. Wall Shear Stress

Fig. 3 and 4 illustrate the evolution of the axial and transverse wall shear stresses along the perimeter of the central cross-section (see Fig. 1) over time. The lower y-axis limit corresponds to the time of maximum inlet pressure.

The axial wall shear stress (AWSS) increases by about one order of magnitude from 0.125 to $256\,\mathrm{Hz}$ in all geometries. Its direction changes with the axial flow direction. In the toroidal and helical ducts, the highest axial wall shear stresses are found at the inner wall of the geometry (Υ - Σ) and are about 40% higher than in the twisted duct. For the AWSS it is the toroidal aspect of the geometry that dominates.

We define counterclockwise (Φ-Υ-Σ-H-Φ) transverse wall shear stress (TWSS) as positive. By opposition to the AWSS, the patterns of the twisted duct dominate the TWSS in the helical duct. In the presence of torsion, strong TWSS emerges close to the corners, which increase and move closer to the corners for higher Womersley numbers. The highest TWSS can be observed in the helical duct close to the corners Υ and Σ.

Fig. 5 displays the ratio of the maximum transverse wall shear stress to the average axial wall shear stress as a function of the Womersley number α. We chose this ratio to quantify the deviation of shear stress from the axial direction, which could be relevant for transverse membrane deflections in the cochlea [15]. The maximum relative wall shear stress in the twisted and helical geometries increases up to 10% and 20%, respectively. Over the entire frequency range, the helical geometry exhibits approximately a two-fold increase in the maximum relative TWSS compared to the twisted duct. Conversely, we observed that the maximum TWSS in the toroidal geometry decreases with α^{-2} and falls below 0.01%.
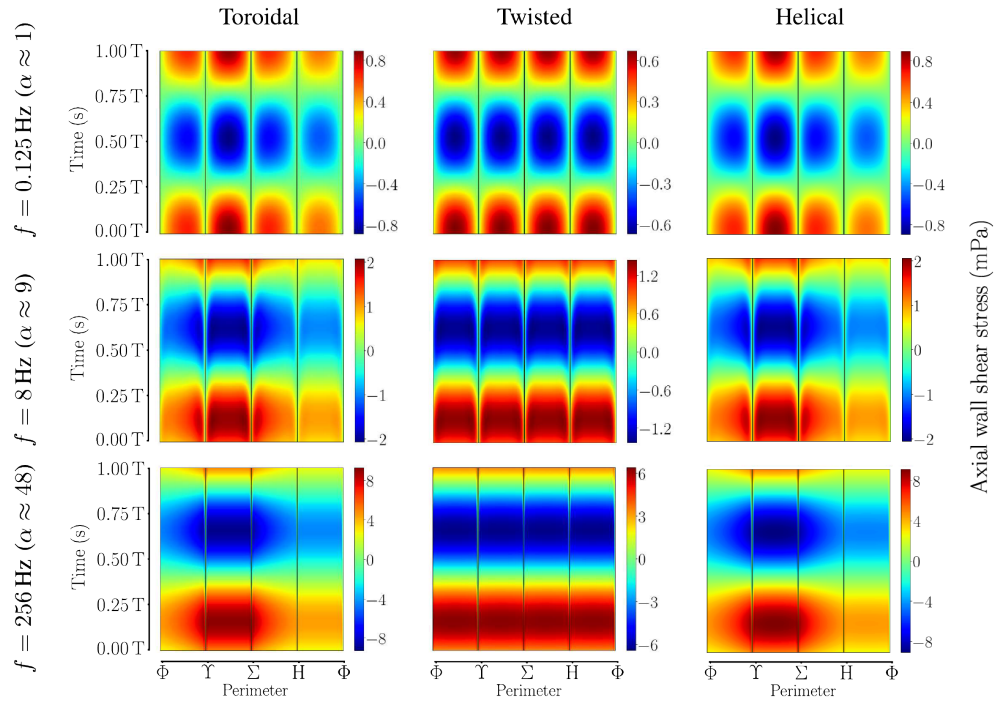
Fig. 3. Axial wall shear stress $\tau_{w,ax}$ visualized for different oscillation frequencies f along the perimeter of the central cross-section. One oscillation period ($T = 1/f$) is shown on the y-axis. Greek capital letters indicate the position along the perimeter. The colorbars are scaled differently.
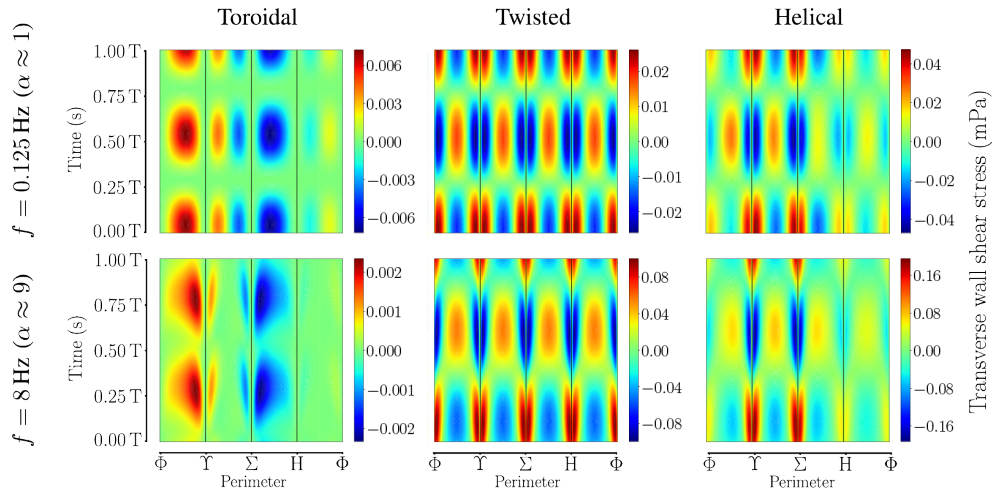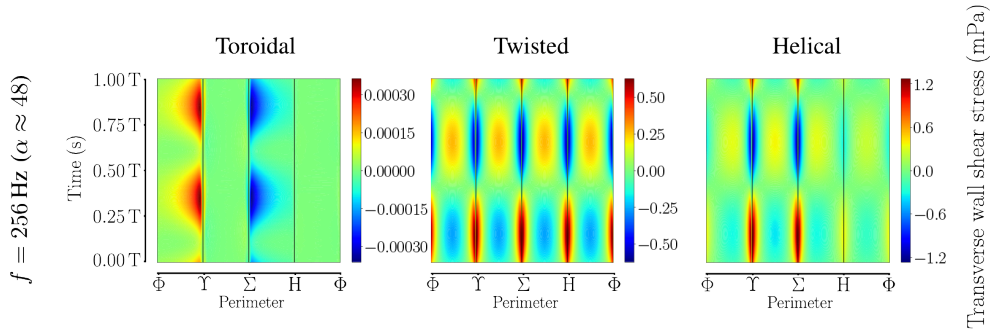

Fig. 4. Continued on next page.

Fig. 4. Transverse wall shear stress $\tau_{w,tr}$ visualized for different oscillation frequencies f along the perimeter of the central cross-section. One oscillation period ($T = 1/f$) is shown on the y-axis. Greek capital letters indicate the position along the perimeter. The colorbars are scaled differently.
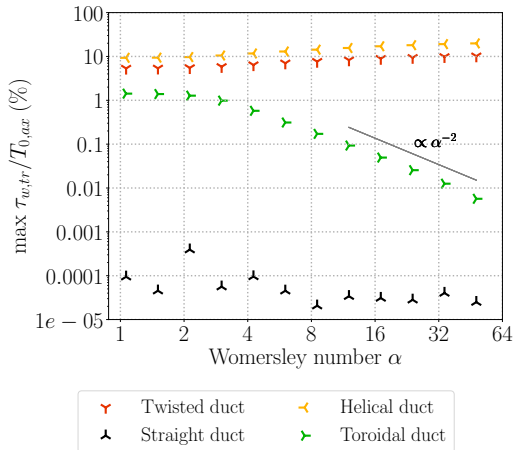

Fig. 5. Maximum transverse wall shear stress $\tau_{w,tr}$ with respect to the mean axial wall shear stress amplitude $T_{0,ax}$ (in percent) as a function of the Womersley number. The black symbols indicate numerical noise defined as the maximum relative transverse wall shear stress found in the straight duct simulations.

IV. DISCUSSION

A. Wall Pressure

Wall pressure fluctuations drive transverse flows near walls, as observed, e.g., in the formation of Dean cells in toroidal ducts [16]. The pressure fluctuations we found reflect the behavior of the transverse flows found by [1], [2]. In helical ducts, torsional effects are dominant for transverse flows at low Reynolds numbers [1] and, as our results suggest, also for the corresponding wall pressure fluctuations. Both are similar to those observed in twisted ducts.

We identified two regimes in Fig. 2 (and Fig. 5): For Womerlsey numbers below 4, the maximum magnitudes behave similarly in the curved, twisted and helical geometries. For $\alpha > 4$ transient inertial forces are predominant and the magnitudes diverge strongly. This coincides with the phase lag between the pressure and the axial velocity which reaches about 90° at $\alpha \approx 4$ [2]. The increase with α^2 in Fig. 2a in helical and twisted ducts can probably be attributed to the unsteady term in the Navier-Stokes equations, which scales with α^2 when written in dimensionless form. Conversely, the magnitudes in the toroidal duct remain nearly constant in Fig. 2a. This could indicate that the non-linear inertial term continues to dominate in the toroidal duct.

B. Wall Shear Stress

The shear stress is highest along the axial direction, but when torsion is present, there is also an evident transverse component. This is an effect of transverse velocities, which in helical ducts at 256 Hz reach a magnitude of above 31% of the main flow [2]. Gammack and Hydon suggested that, for steady flows, torsion leads to an increase in TWSS through altering the transverse flows [3].

Interestingly, the axial shear stress in helical ducts is dominated by curvature, while torsion dominates the transverse component. It seems that

AWSS follows axial flow, while TWSS is affected by transverse flow, which show similar dependencies on geometry [2].

The maximum TWSS in helical duct reaches higher magnitudes than we would expect from a superposition of the effects in twisted and toroidal ducts. This is most evident at $256\,\text{Hz}$, where the transverse shear stress in the helical duct reaches a maximum of 20% of the mean AWSS, while the sum of the TWSS in twisted and toroidal ducts would only amount to 10%. Curvature shifts the axial velocity peak towards the inner wall (low Re, high κ) [14], which enhances transverse velocities there and thus also TWSS caused by torsion. Summarized, the combination of curvature and torsion, as observable in the cochlea, enhance TWSS, while curvature alone leads to negligible TWSS.

C. Potential Physiological Implication

The geometry induced transverse flow introduces wall shear stress and local pressure fluctuations which have magnitudes that could be physiologically relevant, especially in the presence of torsion and close to corners. This is particularly interesting because in the cochlea the axial flow and its corresponding transverse flows occur mainly in the scala tympani and vestibuli, introducing possibilities of fluid-structure interactions. Membrane deformations could lead to radial or transverse flow phenomena within the interfacing scala media, which contains the sensory epithelium for hearing.

D. Study Limitations

The main limitation of our study is the use of abstract geometries to represent the highly complex anatomy of the human cochlea [17]. Further studies that include fluid-membrane interactions are needed to investigate the possible effects on the mechanics of the cochlea.

REFERENCES

[1] C. J. Bolinder, "First- and higher-order effects of curvature and torsion on the flow in a helical rectangular duct," *Journal of Fluid Mechanics*, vol. 314, pp. 113–138, 1996.

[2] N. Harte, D. Obrist, M. Caversaccio, G. P. R. Lajoinie, and W. Wimmer, "Transverse flow under oscillating stimulation in helical square ducts with cochlea-like geometrical curvature and torsion," arXiv preprint arXiv:2303.15603, 2023.

[3] D. Gammack and P. E. Hydon, "Flow in pipes with non-uniform curvature and torsion," *Journal of Fluid Mechanics*, vol. 433, 2001.

[4] C. Cox, M. R. Najjari, and M. W. Plesniak, "Three-dimensional vortical structures and wall shear stress in a curved artery model," *Physics of Fluids*, vol. 31, no. 12, 2019.

[5] H. Felix, A. D. Fraissinette, L.-G. Johnsson, and M. J. Gleeson, "Morphological features of human reissner's membrane," *Acta oto-laryngologica*, vol. 113, no. 3, pp. 321–325, 1993.

[6] W. Wimmer, L. Anschuetz, S. Weder, F. Wagner, H. Delingette, and M. Caversaccio, "Human bony labyrinth dataset: Co-registered ct and micro-ct images, surface models and anatomical landmarks," *Data in brief*, vol. 27, p. 104782, 2019.

[7] H. Rask-Andersen, W. Liu, E. Erixon, A. Kinnefors, K. Pfaller, A. Schrott-Fischer, and R. Glueckert, "Human cochlea: anatomical characteristics and their relevance for cochlear implantation," *The Anatomical Record: Advances in Integrative Anatomy and Evolutionary Biology*, vol. 295, no. 11, pp. 1791–1811, 2012.

[8] P. Aebischer, M. Caversaccio, and W. Wimmer, "Fabrication of human anatomy-based scala tympani models with a hydrophilic coating for cochlear implant insertion experiments," *Hearing research*, vol. 404, p. 108205, 2021.

[9] P. K. Kundu, I. M. Cohen, and D. R. Dowling, "Chapter 3 - kinematics," in *Fluid Mechanics*, sixth edition ed., P. K. Kundu, I. M. Cohen, and D. R. Dowling, Eds. Boston: Academic Press, 2016, pp. 77–108.

[10] C. R. Steele and S. Puria, "Cochlear Mechanics," in *The Biomedical Engineering Handbook*, 4th ed., J. D. Bronzino and D. R. Peterson, Eds. Biomedical Engineering Fundamentals, 2014, ch. 24.

[11] N. T. Greene, H. A. Jenkins, D. J. Tollin, and J. R. Easter, "Stapes displacement and intracochlear pressure in response to very high level, low frequency sounds," *Hearing Research*, vol. 348, 2017.

[12] M. Koch, T. Eßinger, H. Maier, J. Sim, L. Ren, N. Greene, T. Zahnert, M. Neudert, and M. Bornitz, "Methods and reference data for middle ear transfer functions," *Scientific reports*, vol. 12, no. 1, pp. 1–17, 2022.

[13] H. S. Kheshgi, "Laminar flow in twisted ducts," *Physics of Fluids A*, vol. 5, 1992.

[14] A. Pantokratoras, "Steady laminar flow in a 90° bend," *Advances in Mechanical Engineering*, vol. 8, no. 9, pp. 1–9, 2016.

[15] N. Ciganović, A. Wolde-Kidan, and T. Reichenbach, "Hair bundles of cochlear outer hair cells are shaped to minimize their fluid-dynamic resistance," *Scientific Reports*, vol. 7, no. 1, pp. 1–9, 2017.

[16] W. R. Dean, P. Character, and N. Nov, "Fluid Motion in a Curved Channel," *Society*, vol. 121, no. 787, pp. 402–420, 1928.

[17] A. De Paolis, H. Watanabe, J. T. Nelson, M. Bikson, M. Packer, and L. Cardoso, "Human cochlear hydrodynamics: A high-resolution μCT-based finite element study," *Journal of Biomechanics*, vol. 50, pp. 209–216, 2017.